RSC Advances

PAPER

View Article Online
View Journal | View Issue

# Far-infrared optical constants of ZnO and ZnO/Ag nanostructures

Cite this: *RSC Adv.*, 2014, **4**, 20902

Reza Zamiri,*[a] Avito Rebelo,[a] Golriz Zamiri,[b] Atena Adnani,[c] Ajay Kuashal,[a] Michael Scott Belsley[d] and J. M. F. Ferreira[a]

Received 22nd February 2014
Accepted 25th April 2014

DOI: 10.1039/c4ra01563k

www.rsc.org/advances

We report on the synthesis of ZnO nanoplates and ZnO nanoplate/Ag nanoparticle heterostructures *via* a simple and cost effective wet chemical precipitation method. The prepared samples were characterized for structural and optical properties by X-ray diffraction (XRD), Scanning Electron Microscopy (SEM), UV-VIS reflectance, Raman, and FT-IR spectroscopy. The Kramers Kronig (K K) method and classical dispersion theory was applied to calculate the far-infrared optical constants such as, refractive index $n(\omega)$, dielectric constant $\varepsilon(\omega)$, transverse optical phonon (TO) and longitudinal (LO) optical phonon modes. We determined various optical constant values $n(\omega)$ and $\varepsilon(\omega)$ for ZnO nanostructures in the range of 0 to 9 and 0 to 70, respectively. Whereas, for Ag deposition on ZnO nanostructures, the corresponding $n(\omega)$ and $\varepsilon(\omega)$ values were found to be increased in the range of 0 to 30 and 0 to 800, respectively. The TO and LO optical phonon modes of ZnO nanoplate/Ag nanoparticle heterostructures were also found to be higher (416 cm $^{1}$, 620 cm $^{1}$) when compared with corresponding values obtained for ZnO nanoplates (415 cm $^{1}$, 604 cm $^{1}$).

## A Introduction

Recently, semiconductor/metal composite materials have attracted wide scientific and technological interest due to their unique electrical, optical and catalytic properties, which in turn make them suitable candidates for potential applications in optoelectronic devices.[1 5] ZnO is a wide band gap (3.37 eV at room temperature) semiconductor, and has been studied by numerous researchers during the past 20 years.[6 10] Metals such as Ag and Au have electron storage properties which consecutively make possible to develop charge separation in semiconductor/metal composite systems.[3 5] The suitability of ZnO/Ag based composites for photovoltaic devices has stimulated great interest in the preparation and characterization of this material. In ZnO/Ag heterostructures, Ag displays sharp surface plasmon resonance peak in the visible region of electromagnetic spectra with a favorable frequency dependence of the real and imaginary parts of the dielectric function.[11 14] By reducing size of composite material to nano-scale can change optical properties of materials such as optical dispersion, transmission and reflection *via* scattering and interference.[15,16] Searching new routes for synthesis and processing of nano-scale heterostructures and understanding the relationship between the structures and the properties are part of an emerging and rapidly growing field of nanotechnology.[17 21] There are reports on synthesis of ZnO/Ag heterostructures with different morphologies such as Ag/ZnO nanofibers, Ag/tetrapod-like ZnO whisker nanocompounds, Ag nanoparticles-stabilized ZnO nanosheets and Ag nanoparticles/ZnO nanorods.[22 24] Core/shell Ag/ZnO and ZnO/Ag nanostructures have also been derived from various routes.[25 27] In addition, deposition of Ag nanoparticles onto pre-synthesized ZnO nanorods leads to an enhancement of Raman signals and photocatalytic activity.[28,29] The evaluation of optical constants of ZnO based heterostructures is of considerable importance for applications in integrated optic devices such as switches, filters and optical testers, *etc.*, where the refractive index of a material is the key parameter for device design. The limited degree of precision in optical devices is due to variation in optical properties of a material, including, most specifically, the real and the imaginary parts of the effective complex index of refraction, commonly known as effective optical constants $n(\omega)$ and $k(\omega)$.[30] Precise information on optical properties of ZnO/Ag nanocomposite such as dielectric response to electromagnetic waves in infrared region is essential importance and much desired.

Earlier we have reported on synthesis of ZnO/Ag core/shell nanocomposite by laser ablation technique in liquid media, in which ZnO nanoparticles act as the core and Ag acts as the shell.[10] In the present study, ZnO nanoplates/Ag nanoparticles heterostructure have been grown *via* a simple and cost effective chemical route. Novelty of our chemical route approach is synthesis of complex ZnO/Ag nanostructures without any need

[a]*Department of Materials Engineering and Ceramic, University of Aveiro, Campus Santiago, 3810 193 Aveiro, Portugal. E mail: zamiri.r@gmail.com*

[b]*School of Civil Engineering, K.N. Toosi, University of Technology, Tehran, Iran*

[c]*Department of Analytical Chemistry, Faculty of Chemistry, University of Mazandaran, Babolsar, Iran*

[d]*CFUM, Department of Physics, University of Minho, 4710 059, Braga, Portugal*

of growth template. It is demonstrated that this chemical route is a viable option to obtain ZnO/Ag nano scale heterostructures with good optical properties which will further benefits material research and optoelectronic device applications. The optical properties of the synthesized ZnO/Ag nanocomposites has been systematically investigated in far infrared region as infrared spectroscopy is provide insight into dynamical process related to phonons, charge carriers, spin and their coupling process.

## B Experimental

ZnO nanoplates were prepared by a wet chemical precipitation method. Firstly, 3.352 g of $ZnCl_2$ (Aldrich, Germany) was dissolved in distilled water. The obtained solution was dropped into 100 mL of 0.1 M NaOH (Merk, Germany) solution. For the synthesis of the ZnO/Ag nanostructures, 0.01 M Ag $(NO_3)$ (Aldrich, Germany) was added in vessel containing precipitated ZnO nanostructures. The obtained solution was further stirred for 2 h. Thereafter, $NaBH_4$ solution of 0.1 M was added in stirred solution as a reducing agent to convert Ag ions into Ag particles. The resulting mixture was further kept under continuous stirring for 2 h. The pH value of the solutions was kept nearly in the range of 13–14. Finally in order to obtain the solid phase separation from the liquid phase, the precipitated materials in suspensions were ultra-centrifuged (10 000 rpm, 10 min) to obtain clear supernatant liquids. The obtained solid phases (both ZnO nanoplates and ZnO/Ag nanostructures) were then washed thoroughly in distilled water to remove the unwanted ions ($Na^+$, $Cl^-$, $NO_3^-$). Washing solid precipitates was repeated several times up to getting a $Na^+$ concentration below to 0.66 ppm measured by atomic absorption spectroscopy, followed by drying at 80 °C for 24 h. The structure and morphology of the samples were studied by X-ray diffraction (Shimadzu XRD-6000, Tokyo, Japan) and Scanning Electron Microscopy (SEM, SU-70, Hitachi), respectively. The optical properties of the samples were measured by using UV-visible (Perkin-Elmer, Lambda 35), Raman and FT-IR spectrometry.

## C Results and discussions

Fig. 1 shows the XRD patterns of ZnO and ZnO/Ag nanostructures. The XRD pattern of ZnO shows the presence of a well crystalline hexagonal wurtzite phase (JCPDS, no. 36-1451), whereas, ZnO/Ag nanostructure exhibits the ZnO wurtzite phase and three additional peaks at 38.1°, 44.2° and 64.4° related to (1 1 1), (2 0 0) and (2 2 0) planes of Ag nanoparticles corresponding to face-centered cubic (fcc) metallic Ag phase (JCPDS no. 04-0783). Appearance of Ag peaks in the XRD diffraction pattern clearly confirmed the formation of crystalline silver nanoparticles.

The morphologies of the prepared nanostructures were further studied from SEM analysis. Fig. 2 shows SEM images of ZnO nanostructures (Fig. 2a), and ZnO/Ag nanostructures (Fig. 2b–d). Nano-sized plate like structures has been obtained for both ZnO and ZnO/Ag composites. However, distribution of Ag particles all over the surfaces of ZnO nanoplates has been observed in ZnO/Ag nanocomposites samples (as shown in

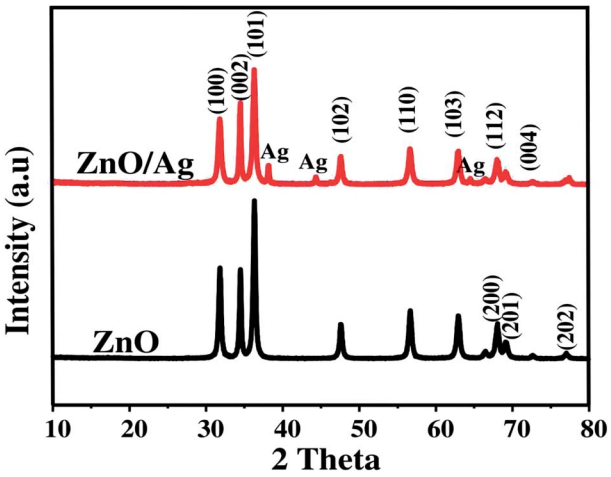


Fig. 1 XRD patterns of ZnO and ZnO/Ag nanostructures.

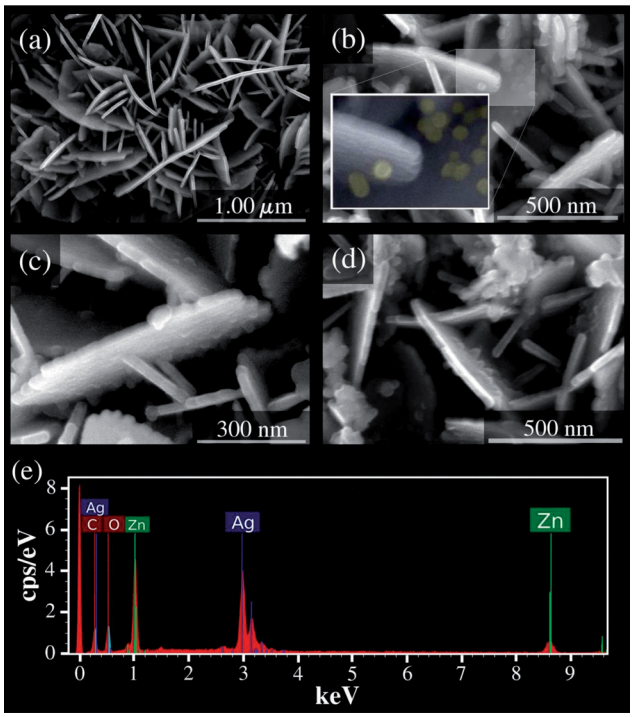


Fig. 2 SEM images of (a) ZnO, (b d) ZnO/Ag nanostructures and (e) EDS analysis of ZnO/Ag nanostructures.

Fig. 2b–d). The presence of Ag content was further confirmed by EDS analysis of ZnO/Ag nanostructures. The obtained EDS spectra are shown in Fig. 2e which shows the presence of Ag, Zn and O in the final products. The absence of extra impurity peaks in EDS spectra suggests the purity of obtained nanostructures with no sign of any additives left in final obtained solid precipitates.

Fig. 3 shows the reflectance spectra of prepared ZnO and ZnO/Ag nanostructures in UV-VIS range of electromagnetic wavelengths. An abrupt change in reflectance behaviour at a wavelength around 385 nm was observed in both the samples, which is assigned to recombination of electron holes in ZnO. In

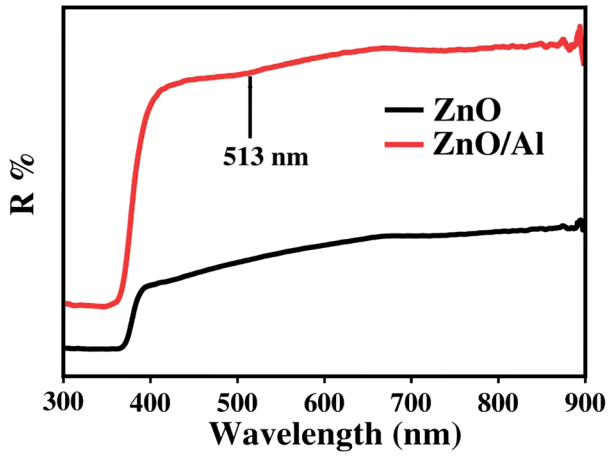


Fig. 3 Reflectance spectra of ZnO and ZnO/Ag nanostructures in visible range of electromagnetic wavelengths.

addition, the specific surface plasmon resonance absorption peak of Ag nanoparticles was also observed at around 513 nm as shown in ZnO/Ag nanostructures reflectance behavior.

The surface plasmon peak location of a metal can be calculated by the following equation.[31]

$$\lambda_p = [4\pi^2 c^2 m_{eff}\varepsilon_0/Ne^2]^{1/2} \quad (1)$$

where, $m_{eff}$ and $N$ are the effective mass and electron density respectively. Red shift in surface plasmon resonance peak has been observed as usually it is at ~400 nm for Ag.[32,33] The observed red shift in surface plasmon resonance peak indicating reduction in electron density of Ag in ZnO/Ag nanostructures. This reduction can be explained according to the Fermi energy levels of ZnO and Ag, as the ZnO work function (4.3 eV) is larger than Ag (4.1 eV), therefore the Fermi level of ZnO is located lower to Ag Fermi level. This leads to easy electrons transfer from Ag nanoparticles to ZnO nanoplates, when the two systems are not in equilibrium.

Fig. 4 indicates the Raman spectra of prepared ZnO and ZnO/Ag nanostructures excited by $\lambda = 1064$ nm laser source. Two strong peaks were found for ZnO and ZnO/Ag nanostructures located at 430 $cm^{-1}$ and 580 $cm^{-1}$ corresponding to E2 and E1(LO) modes of wurtzite ZnO structure respectively.[34] The 437 $cm^{-1}$ peak disappears in ZnO/Ag nanostructure due to overlapping with other stronger resonant Raman scattering peaks. It can be clearly seen that the peaks intensity of ZnO/Ag nanostructure is higher than that observed for ZnO nanostructure. There are two theories which can be applied to explain the enhancement of the peak intensity on Ag deposition on ZnO nanoplates as: (1) the electromagnetic theory which is based on the excitation of localized surface plasmons; (2) chemical theory which rationalizes the effect through the formation of charge transfer complexes and only applies for species which have formed a bond with the surface. The Raman intensity is relative to the intensity of the locally formed *E*-field which can interact with optical phonons and enhances the scattering intensity of active phonons.[31] Therefore, the enhancement of Raman intensity for ZnO/Ag nanostructures is due to strong local *E*-field at the interface between ZnO and Ag. The intensity of interaction among ZnO and Ag is determined by the polarization induced in each one due to the *E*-field arising from the charge separation, as the positive ions left on the Ag nanoparticles surface after electrons transfer to the ZnO.

Fig. 5 shows FT-IR spectrum of ZnO and ZnO/Ag nanostructures. The strong absorption band ranging from 400 $cm^{-1}$ to 500 $cm^{-1}$ is assigned to Zn–O stretching vibration mode of the ZnO nanoplates and intensity of this peak is reduced after formation of Ag nanoparticles on the surface of ZnO nanoplates.[35] There are also broad peaks at 3450 $cm^{-1}$ and 1630 $cm^{-1}$, corresponding to the hydroxyl groups due to the adsorption of water on the particles surface.[36] No vibration mode in relation with Ag was observed in the spectrum of ZnO/Ag nanostructure, which indicates that there is no chemical bonding between Ag and ZnO.

The K–K method was applied on FT-IR reflectance spectra data to evaluate the far-inferred optical constants of the prepared ZnO and ZnO/Ag nanostructures. . The experimentally measured reflectance spectra of ZnO and ZnO/Ag nanostructures are shown in Fig. 6. The reflective index $n$ is an

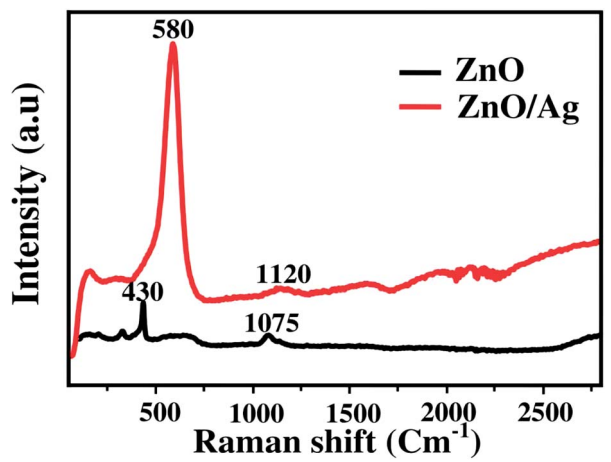


Fig. 4 Raman spectra of the ZnO and ZnO/Ag nanostructures.

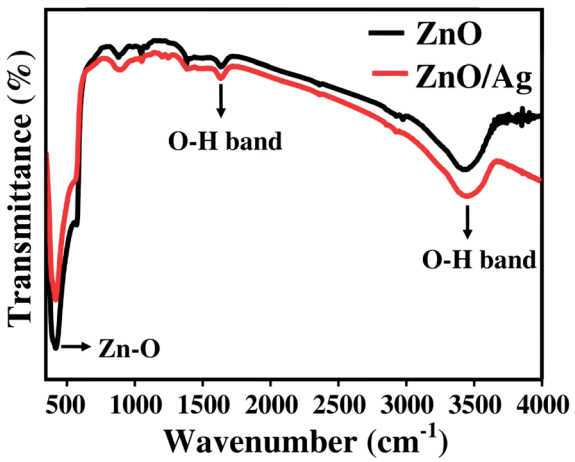


Fig. 5 FT-IR spectrum of ZnO and ZnO/Ag nanostructures.

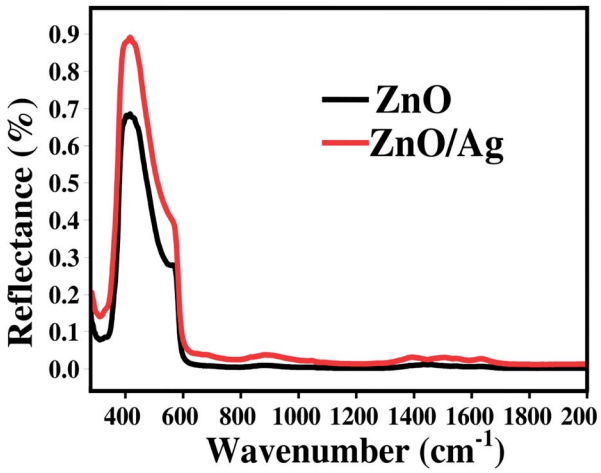


Fig. 6 Reflectance spectra of ZnO and ZnO/Ag nanostructures.

important physical quantity in optical design and generally is a complex quantity:

$$\tilde{n}(\omega) = n(\omega) + ik(\omega) \quad (2)$$

where $n(\omega)$ and $k(\omega)$ are the real and the imaginary parts of the complex refractive index respectively, and can be obtained by the following equations:[37]

$$n(\omega) = (1 \quad R(\omega))\Big/\Big(1 + R(\omega) \quad 2\sqrt{(R(\omega))}\Big)\cos\varphi(\omega) \quad (3)$$

$$k(\omega) = \Big(2\sqrt{(R(\omega))}\cos(\varphi)\Big)\Big/\Big(1 + R(\omega) \quad 2\sqrt{(R(\omega))}\Big)\cos\varphi(\omega) \quad (4)$$

Here, $\varphi(\omega)$ is the phase change between the incident and the reflected signal at a particular wave number, $\omega$ and $R(\omega)$ is the reflectance in that wave number, $\omega$. The phase change can be calculated from the K–K dispersion relation given by:[38]

$$\varphi(\omega) = (\quad \omega)/\pi\int_0^{\infty}(\ln R(\omega') \quad \ln R(\omega))\Big/(\omega'^2 \quad \omega^2)\mathrm{d}\omega' \quad (5)$$

This integral can further be precisely evaluated by using Maclaurin's method as:[39]

$$\varphi(\omega_j) = (4\omega_j/\pi)\Delta\omega\sum_i\Big(\ln\Big(\sqrt{R(\omega)}\Big)\Big/\Big(\omega_i^2 \quad \omega_j^2\Big)\Big) \quad (6)$$

here $\Delta\omega = \omega_{j+1} \quad \omega_j$ and if $j$ is an even number then $i = 1, 3, 5, 6,..j \quad 1, j+1,...$ while, if $j$ is an odd number then $i = 2, 4, 6,..j \quad 1, j+1,...$

In addition, the dielectric function can be obtained by the square of the refractive index. Therefore, the real and imaginary parts of the complex dielectric function are given by:

$$\begin{aligned}\varepsilon = [\tilde{n}(\omega)]^2 &= [n(\omega) + ik(\omega)]^2 \Rightarrow \varepsilon' + i\varepsilon'' \\ &= n^2(\omega) \quad k^2(\omega) + 2in(\omega)k(\omega) \Rightarrow \{\varepsilon'(\omega) \\ &= n^2(\omega) \quad k^2(\omega);\ \varepsilon''(\omega) = 2n(\omega)k(\omega)\end{aligned} \quad (7)$$

The calculated optical constant values of ZnO and ZnO/Ag nanostructures obtained using eqn (2)–(7) are shown in Fig. 7a and b. The strong peaks were observed for $n(\omega)$ and $k(\omega)$ at around 415 $cm^{-1}$ and 410 $cm^{-1}$, respectively. However, the intensity of the peaks for both $n(\omega)$ and $k(\omega)$ increased from $n_{max}$ = 8.80, and $k_{max}$ = 4.16 (for ZnO nanostructures) to $n_{max}$ = 28.80, $k_{max}$ = 13.30 (for ZnO/Ag nanostructures). This increase

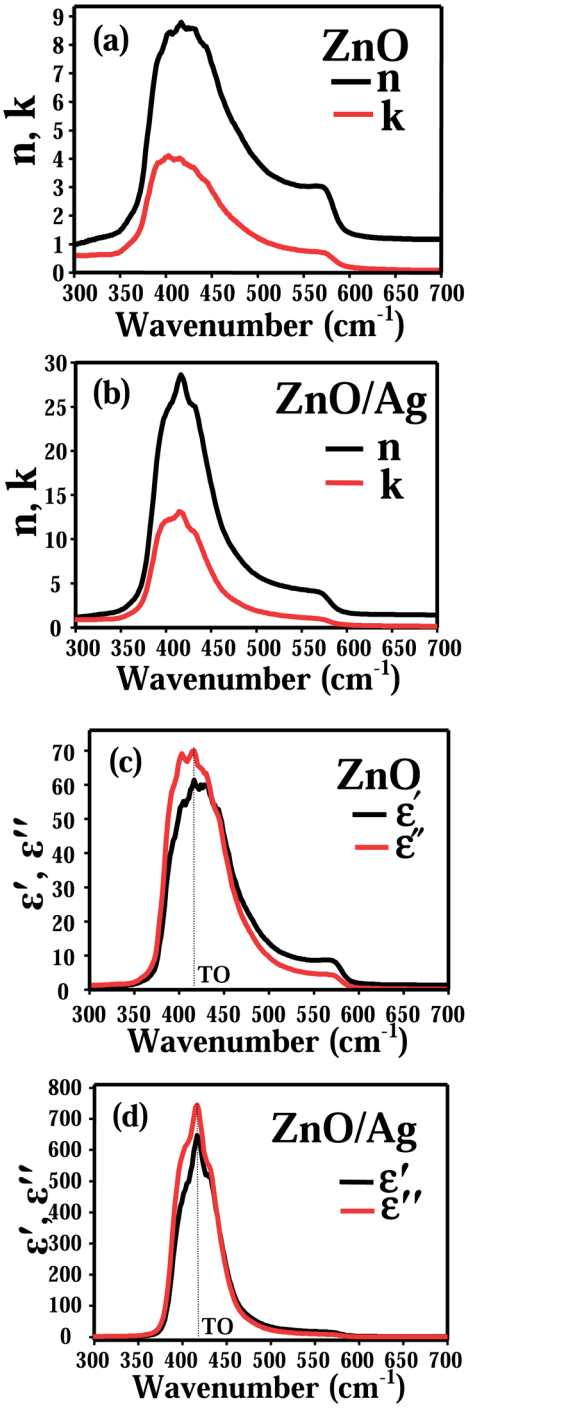


Fig. 7 (a and b) Refractive index and extinction coefficient, (c and d) real and imaginary parts of dielectric functions of ZnO and ZnO/Ag nanostructures.

in intensity values could be due to the formation of Ag nanoparticles on the surface of ZnO nanoplates which causes the reduction of the Zn–O absorption band intensity in the far infrared region. The calculated values of real and imaginary parts of the dielectric function of the prepared samples are also shown in Fig. 7c and d. It can be seen that the value of maximum dielectric function was drastically increased for ZnO/Ag nanostructures compared to ZnO nanostructures. Therefore, it can be concluded that the presence of Ag nanoparticles on the surface of ZnO nanoplate can improve optical properties of ZnO in far infrared region.

Till date, there are certain reports on optical properties of bulk and nanostructured ZnO in infrared region and the field is still wide open as per its potential in device application.[40 47] For example, García-Serrano *et al.*[41] used far infrared (FIR) reflectance spectra for the qualitative determination of free carrier density in metal and semiconductor nanoclusters embedded ZnO films. On the other hand, Yamamoto *et al.*[42] focused on the optical surface phonon modes in small ZnO crystals using FIR transmission measurements at room temperature. In addition, terahertz time-domain spectroscopy was used to determine refractive index, dielectric constant and absorption coefficient of bulk and nanostructured ZnO in the FIR region and it was found that ZnO nanostructures exhibit very similar phonon resonances with that of single-crystal ZnO.[44,45] Polarized FIR reflectance technique has also been applied by researchers to study the optical properties of pure and Mn doped ZnO nanoparticles prepared by sol gel method.[47] They report optical constant values *i.e.* refractive index ($n$) and dielectric constants ($\varepsilon$) values in the range between 1 to 7 and 25 to 35, respectively. We determined various optical constants values $n$ and ε for ZnO nanostructures in the range of 0 to 9 and 0 to 70, respectively. However, on Ag deposition on ZnO nanostructures, the corresponding $n$ and $\varepsilon$ values were found to be increase in the range of 0 to 30 and 0 to 800, respectively.

Table 1 Various TO and LO optical phonons values of ZnO and ZnO/Ag nanostructures

| Samples | Transfer optical phonon (TO), cm $^{1}$ | Longitude optical phonon (LO), cm $^{1}$ |
|---|---|---|
| ZnO | 415 | 604 |
| ZnO/Ag | 416 | 620 |

The TO and LO modes of a material are useful to illustrate the optical interactions with the lattice. TO mode frequencies corresponds to the frequency at which imaginary part of the dielectric function shows a peaks (Fig. 7c and d).[48] The LO mode frequencies can be obtained by plotting the imaginary part of $1/\varepsilon$ behaviour against wave number as shown in Fig. 8a and b. Frequency at which peak observed in Fig. 8, corresponds to LO mode frequency. Table 1 illustrates various TO and LO optical phonons values obtained for prepared ZnO and ZnO/Ag nanostructures.

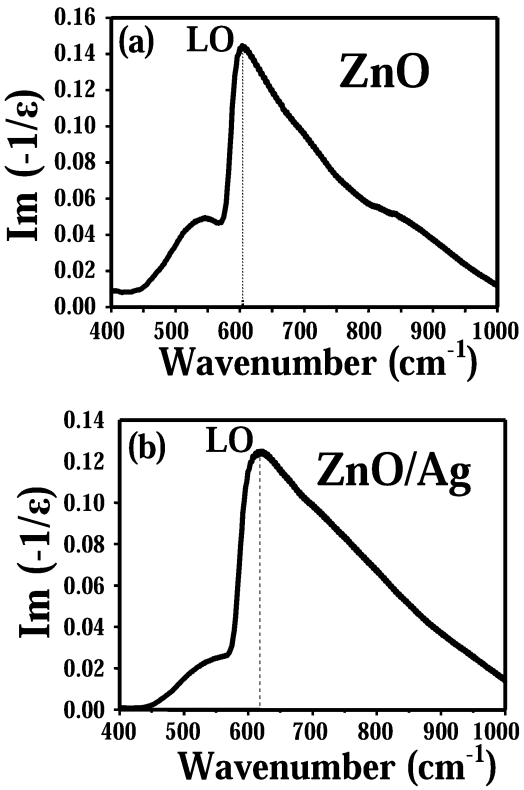


Fig. 8 Imaginary part of behaviour with wave number for ZnO and ZnO/Ag nanostructures.

## D Conclusions

ZnO nanoplates and ZnO nanoplates/Ag nanoparticles heterostructures have been successfully synthesized *via* cost effective wet precipitation method. The presence of Ag in ZnO/Ag nanocomposites was confirmed by the presence of extra phases along with wurtzite ZnO phase in XRD spectra and by taking EDS spectra. Nano-sized plates like structure were observed in SEM images of the prepared samples. An absorption peak observed in reflectance spectra of ZnO/Ag sample at a wavelength of ~513 nm corresponds to surface Plasmon resonance of Ag nanoparticles. Raman peak intensity was found to be higher in case of ZnO/Ag nanostructures when compared with Raman intensity observed for ZnO nanostructures. The far-infrared optical constants of the prepared samples were successfully calculated by using Kramers–Kronig method. far infrared optical properties of ZnO nanoplates were found to enhance when Ag is deposited on surface of ZnO nanoplates making it as ZnO/Ag nanocomposites. The enhancement in optical properties of ZnO will further benefit its potential use in various optical devices.

## Acknowledgements

Authors, Reza Zamiri and A. Kaushal would like to thank the Foundation for Science and Technology of Portugal (FCT) for the financial support under the grant references, SFRH/BPD/76185/2011 and SFRH/BPD/77598/2011, respectively. The

 

authors would also like to thank CICECO for the work at the University of Aveiro.

## Notes and references

1 G. Merga, *et al.*, Probing silver nanoparticles during catalytic $H_2$ evolution, *J. Am. Chem. Soc.*, 2008, **130**(22), 7067–7076.
2 J.-s. Choi, *et al.*, Biocompatible heterostructured nanoparticles for multimodal biological detection, *J. Am. Chem. Soc.*, 2006, **128**(50), 15982–15983.
3 K. Sun, *et al.*, Solution synthesis of large-scale, high-sensitivity ZnO/Si hierarchical nanoheterostructure photodetectors, *J. Am. Chem. Soc.*, 2010, **132**(44), 15465–15467.
4 X. Li and Y. Wang, Structure and photoluminescence properties of Ag-coated ZnO nano-needles, *J. Alloys Compd.*, 2011, **509**(19), 5765–5768.
5 R. K. Sahu, *et al.*, Stabilization of intrinsic defects at high temperatures in ZnO nanoparticles by Ag modification, *J. Colloid Interface Sci.*, 2012, **366**(1), 8–15.
6 R. Zamiri, *et al.*, Er doped ZnO nanoplates: Synthesis, optical and dielectric properties, *Ceram. Int.*, 2014, **40**(1), 1635–1639.
7 R. Zamiri, *et al.*, Effects of rare-earth (Er, La and Yb) doping on morphology and structure properties of ZnO nanostructures prepared by wet chemical method, *Ceram. Int.*, 2013, **40**, 523–529.
8 R. Zamiri, *et al.*, Electrical properties of Ag-doped ZnOnano-plates synthesized *via* wet chemical precipitation method., *Ceram. Int.*, 2014, **40**(3), 4471–4477.
9 R. Zamiri, *et al.*, Aqueous starch as a stabilizer in zinc oxide nanoparticle synthesis *via* laser ablation, *J. Alloys Compd.*, 2012, **516**, 41–48.
10 R. Zamiri, *et al.*, Laser assisted fabrication of ZnO/Ag and ZnO/Au core/shell nanocomposites, *Appl. Phys. A: Solids Surf.*, 2013, 1–7.
11 Y. Yin, W. Que and C. Kam, ZnO nanorods on ZnO seed layer derived by sol–gel process, *J. Sol-Gel Sci. Technol.*, 2010, **53**(3), 605–612.
12 Y. Sun, *et al.*, Synthesis of aligned arrays of ultrathin ZnO nanotubes on a Si wafer coated with a thin ZnO film, *Adv. Mater.*, 2005, **17**(20), 2477–2481.
13 C. Jiang, *et al.*, Improved dye-sensitized solar cells with a ZnO-nanoflower photo anode, *Appl. Phys. Lett.*, 2007, **90**(26), 263501–263501.
14 J. Elias, *et al.*, Conversion of ZnO nanowires into nanotubes with tailored dimensions, *Chem. Mater.*, 2008, **20**(21), 6633–6637.
15 W. Du, *et al.*, Ultrathin β-In2S3 nanobelts: shape-controlled synthesis and optical and photocatalytic properties, *Cryst. Growth Des.*, 2008, **8**(7), 2130–2136.
16 A. B. Panda, *et al.*, Synthesis, assembly, and optical properties of shape-and phase-controlled ZnSe nanostructures, *Langmuir*, 2007, **23**(2), 765–770.
17 H. W. Kim, K. M. Kang and H.-Y. Kwak, Preparation of supported Ni catalysts with a core/shell structure and their catalytic tests of partial oxidation of methane, *Int. J. Hydrogen Energy*, 2009, **34**(8), 3351–3359.
18 P. Yang, *et al.*, Fabrication and luminescent properties of the core–shell structured $YNbO_4$: $Eu^{3+}/Tb^{3+}@SiO_2$ spherical particles, *J. Solid State Chem.*, 2008, **181**(8), 1943–1949.
19 Z. Ma, *et al.*, Synthesis and characterization of multifunctional silica core–shell nanocomposites with magnetic and fluorescent functionalities, *J. Magn. Magn. Mater.*, 2009, **321**(10), 1368–1371.
20 Y. Lu, C.-L. Yan and S.-Y. Gao, Preparation and recognition of surface molecularly imprinted core–shell microbeads for protein in aqueous solutions, *Appl. Surf. Sci.*, 2009, **255**(12), 6061–6066.
21 H. Liu, *et al.*, Electrochemical performance of $LiFePO_4$ cathode material coated with $ZrO_2$ nanolayer, *Electrochem. Commun.*, 2008, **10**(1), 165–169.
22 D. Zhang, X. Liu and X. Wang, Growth and photocatalytic activity of ZnO nanosheets stabilized by Ag nanoparticles, *J. Alloys Compd.*, 2011, **509**(15), 4972–4977.
23 H. Hu, *et al.*, ZnO/Ag heterogeneous structure nanoarrays: Photocatalytic synthesis and used as substrate for surface-enhanced Raman scattering detection, *J. Alloys Compd.*, 2011, **509**(5), 2016–2020.
24 X. Yin, W. Que and F. Shen, ZnO nanorods arrays with Ag nanoparticles on the (002) plane derived by liquid epitaxy growth and electrodeposition process, *Thin Solid Films*, 2011, **520**(1), 186–192.
25 F. Li, *et al.*, Synthesis and characterization of ZnO–Ag core–shell nanocomposites with uniform thin silver layers, *Appl. Surf. Sci.*, 2010, **256**(20), 6076–6082.
26 C. Song, *et al.*, Facile synthesis of Ag/ZnO microstructures with enhanced photocatalytic activity, *Mater. Lett.*, 2010, **64**(14), 1595–1597.
27 Y. Zheng, *et al.*, Ag/ZnO heterostructure nanocrystals: synthesis, characterization, and photocatalysis, *Inorg. Chem.*, 2007, **46**(17), 6980–6986.
28 X. Yin, *et al.*, Ag nanoparticle/ZnO nanorods nanocomposites derived by a seed-mediated method and their photocatalytic properties, *J. Alloys Compd.*, 2012, **524**, 13–21.
29 C. Chen, *et al.*, Enhanced Raman scattering and photocatalytic activity of Ag/ZnO heterojunction nanocrystals, *Dalton Trans.*, 2011, **40**(37), 9566–9570.
30 A. Rakic, *et al.*, Optical properties of metallic films for vertical-cavity optoelectronic devices, *Appl. Opt.*, 1998, **37**, 5271–5282.
31 G. Shan, *et al.*, Enhanced Raman scattering of ZnO quantum dots on silver colloids, *J. Phys. Chem. C*, 2007, **111**(8), 3290–3293.
32 R. Zamiri, *et al.*, Fabrication of silver nanoparticles dispersed in palm oil using laser ablation, *Int. J. Mol. Sci.*, 2010, **11**(11), 4764–4770.
33 R. Zamiri, *et al.*, Laser-fabricated castor oil-capped silver nanoparticles, *Int. J. Nanomed.*, 2011, **6**, 565.
34 H.-M. Cheng, *et al.*, Raman scattering and efficient UV photoluminescence from well-aligned ZnO nanowires epitaxially grown on GaN buffer layer, *J. Phys. Chem. B*, 2005, **109**(18), 8749–8754.

35 J. Das and D. Khushalani, Nonhydrolytic route for synthesis of ZnO and its use as a recyclable photocatalyst, *J. Phys. Chem. C*, 2010, **114**(6), 2544–2550.
36 S. C. Pillai, *et al.*, Synthesis of high-temperature stable anatase $TiO_2$ photocatalyst, *J. Phys. Chem. C*, 2007, **111**(4), 1605–1611.
37 D. C. Harris and M. D. Bertolucci, *Symmetry and Spectroscopy: An Introduction to Vibrational and Electronic Spectroscopy*, DoverPublications. com, 1978.
38 V. Lu carini, *et al.*, *Kramers–Kronig Relations in Optical Materials Research*, 2005, Springer Series in Optical Sciences.
39 M. Ghasemifard, S. Hosseini and G. H. Khorrami, Synthesis and structure of PMN–PT ceramic nanopowder free from pyrochlore phase, *Ceram. Int.*, 2009, **35**(7), 2899–2905.
40 J. Kim, S. Jung, E. J. Choi, K. Kim, K. Lee and S. Im, Infrared spectroscopy of the interface charge in a ZnO field-effect transistor, *Appl. Phys. Lett.*, 2008, **93**(24), 241902.
41 J. García-Serrano, G. Casarrubias-Segura, A. G. Galindo, X. Mathew and U. Pal, Infrared study of free carriers in X/ZnO (X = semiconductor, metal) nanocomposites, *Thin Solid Films*, 2005, **490**(2), 137–141.
42 K. Yamamoto, C.-D. Tran, H. Shimizu and K. Abe, Optical Surface Phonon Modes in ZnO Small Crystals, *J. Phys. Soc. Jpn.*, 1977, **42**(2), 587–590.
43 E. V. Lavrov, Infrared absorption spectroscopy of hydrogen-related defects in ZnO, *Phys. B*, 2003, **340–342**, 195–200.
44 A. K. Azad, J. Han and W. Zhang, Terahertz dielectric properties of high-resistivity single-crystal ZnO, *Appl. Phys. Lett.*, 2006, **88**(2), 021103.
45 J. G. Han, A. K. Azad and W. L. Zhang, Far-infrared characteristics of bulk and nanostructured wide-bandgap semiconductors, *J. Nanoelectron. Optoelectron.*, 2007, **2**(3), 222–233.
46 P. Ooi and S. Lee, Far Infrared Optical Properties of Bulk Wurtzite Zinc Oxide Semiconductor, *J. Mater. Sci. Technol.*, 2011, **27**(5), 465–470.
47 M. E. Abrishami, S. M. Hosseini, E. A. Kakhki, A. Kompany and M. Ghasemifard, Synthesis and structure of pure and mn-doped zinc oxide nanopowders, *Int. J. Nanosci.*, 2010, **09**(01n02), 19–28.
48 S. Ng, Z. Hassan and H. Abu Hassan, Kramers–Kronig analysis of infrared reflectance spectra with a single resonance, *Jurnal Teknologi*, 2012, **44**(1), 67–76.